Development and Study of Small Database for the Activation of Nitrous Oxide Towards Formation of Iron(IV)-Oxo Species

A Thesis Presented for the

Master of Science

Degree

The University of Tennessee, Knoxville

Tobias Barthalomew Robertson

May 2023

To my parents: John and Tamara Robertson who have always supported me in my educational pursuits.

Acknowledgments

Dr. Konstantinos D. Vogiatzis under whose advisement and guidance this work was completed.

Dr. Justin Kirkland whose iron(IV)-oxo database was integral to this work.

National Science Foundation which supported in part this work supported via Grant No. CHE-1800237.

Infrastructure for Scientific Applications and Advanced Computing (ISAAC) maintained by the University of Tennessee which provided the computational resources for this work.

Abstract

Nitrous oxide (N_2O) can undergo an oxygen atom transfer (OAT) reaction resulting in inert nitrogen gas (N_2) while transferring an oxygen atom to a molecular complex or material. This process is of catalytic importance since this OAT reaction can be leveraged to form iron(IV)-oxo sites, which are known to be catalytic intermediates. Here, an investigation of the ligand field effects on primarily iron(II) complexes for the formation of iron(IV)-oxo sites with nitrous oxide as the oxidant is reported. An initial database of sixty-four molecular complexes with ligand environments varying in field strength and coordination geometry was studied using density functional theory (DFT) calculations. Additional structures were also studied to specifically interrogate a trend observed in the initial database while investigating potential predictive descriptors for the OAT reaction barrier. General design principles rooted in the performance of the ligand fields assessed are discussed and have potential applications in catalyst design for both molecular complexes and metal organic frameworks (MOFs).

Table of Contents

List of Figures

List of Attachments

Nitrous Oxide Coordinated Structures (N2O_Structures.txt)

Transition State Structures (TS_Structures.txt)

Chapter 1

Introduction

General Background

Methane functionalization for the synthesis of methanol or light hydrocarbons that can be used as alternative fuels is of significant interest to the petroleum chemistry, as methane is the primary component of natural gas, as well as being important for industrial chemical synthesis. Methane activation via transition metals occurs via several different mechanisms, in nature the use of reactive metal oxygen intermediates is a major mechanism for the functionalization of methane. One such example is methane monooxygenases (MMOs), these are a category of enzymes that convert methane into methanol under ambient conditions using O_2 as the oxidant.[10]

The formation of reactive oxygen species for selective partial oxidation of hydrocarbons such as methane and other light hydrocarbons depends in part on the oxidant utilized. Given the gaseous nature of methane, porous materials such as zeolites and metal-organic frameworks (MOFs) are of significant interest as catalysts for the oxidation of methane. The first zeolite with extraframework Fe centers capable of oxidizing methane to methanol was introduced by Pannov in 1990[13] and recently, the geometric and electronic structure of the reactive oxygen intermediate was reported by Snyder et al.[15] The extraframework Fe(II) forms a Fe(IV)-oxo structure with a distorted axial square pyramidal geometry upon the coordination of N_2O. The

rapid methane oxidation is a result of two factors: the weak ligand field that the Fe center experiences from the oxygen atoms of the framework and the constrained coordination geometry imposed by the rigid zeolitic lattice. Formation and usage of an iron-oxo species in iron zeolites has been studied both computationally and experimentally.[4, 47, 48, 49, 50, 51, 52, 53, 54, 55]

Over the past years, metal-organic frameworks (MOFs) emerged as an alternative to conventional porous materials such as zeolites. MOFs being composed of inorganic nodes (single metal atoms or metal clusters) connected via organic linkers offer the advantages of permanent porosity and a large surface area while also being extremely tunable. The tunability of MOFs arrises from the variety of inorganic nodes and organic linkers that can be used for the synthesis of MOFs, which allows for an extensive number of possible combinations. Due to their unique properties, MOFs with significant stability have been employed for a variety of catalytic applications including oxidation, reduction, electrocatalysis, and photocatalytic reactions.[9] Alkane oxidation in certain MOFs mimicking the C–H functionalization via metal-oxo sites in enzymes and zeolites has been recently explored. Xiao et al.[21] reported that Fe-containing MOF-74 (also known as Fe_2(dobdc), dobdc^{4}-= 2,5-dioxido-1,4-benzenedicarboxylate) and its magnesium diluted (Fe_0.1Mg_1.9(dobdc)) variant catalyze the oxidation of ethane to ethanol using N_2O as the oxidant for the creation of the catalytic iron-oxo species. It was suggested that the Fe(IV)-oxo intermediate is formed at the undercoordinated Fe sites, with a weak ligand field enhancing the highly reactive, high-spin (S = 2) active site which was further verified by theoretical calculations. The proposed reaction mechanism contains five main steps: N_2O coordination to the Fe(II) site, formation of the Fe(IV)-oxo intermediate, C–H bond activation, radical rebound to form ethanol, and desorption of ethanol.[21, 17] This study suggested that the bond dissociation of the N-O bond in N_2O for the Fe(IV)-oxo formation is the rate-determining step of the catalytic cycle. A follow-up study used the O-atom donor barrier in order to estimate if already synthesized Fe-based MOFs can also catalyze the same reaction.[30] A

two-step process was applied to the computational screening of the Computation-Ready Experimental (CoRE) MOF database [39, 40] which included the automated recognition of under-coordinated Fe sites and the computation of the N-O activation barrier, which was used as a descriptor of catalytic activity. Similar considerations were applied in computational studies by the Snurr [28, 41, 42, 3, 43] and Kulik groups [44, 45, 46] for the screening of material and molecular databases for oxidation catalysis. The most recent related work from the Kulik group[46] utilizes nitrous oxide as the oxidant; however, the focus of the work is not the activation of nitrous oxide but rather the C-H activation involving the resultant iron-oxo species. Furthermore, the focus of the study was low and intermediate spin states rather than pursuing high spin species. Thus the focus and goal of the reported research was not to work towards optimization of the activation of nitrous oxide.

Solomon and coworkers[29] developed a methodology for investigating the geometric and electronic structure aspects of non-heme iron based enzyme sites that utilize an iron-oxo intermediate with and octahedral coordination utilizing water as the oxygen donor. Utilizing this methodology it was found that the low spin iron-oxo species present in these cases make use of a π-type channel while the high spin cases have both a π channel and a σ channel.

Kazaryan and Baerends[27] also utilizing octahedral ligand environments compared a weak ligand field ($(H_2O)_5$) to a strong ligand field ($(NH_3)_4$ with and axial H_2O ligand) for iron(IV)-oxo species to interrogate the impact of spin state on the reactivity of these species with respect to hydrogen abstraction. It was found that for both the weak and strong field models the quintet spin state resulted in a lower hydrogen abstraction barrier than the triplet spin state, the ground state spin multiplicity for the weak field was the quintet spin state while the ground state for the strong field was the triplet spin state. Kazaryan and Baerends[27] did not however study the formation of the iron-oxo species in their study.

Nitrous Oxide as Terminal Oxidant

In biological enzymes O_2 and H_2O_2 are often the terminal oxidant for the formation of iron-oxo species and are environmentally benign.[56, 57] Nitrous oxide, which is a known potent greenhouse gas, can also be used as an oxidant to form iron-oxo species[16, 17, 4, 9] while forming environmentally benign and nearly entirely chemically inert N_2. The gaseous nature of nitrous oxide under non-extreme conditions allows for the efficient permeation of porous materials such as MOFs and zeolites. Nitrous oxide can coordinate to a metal center either nitrogen end-on or oxygen end-on but only the latter is desired in order to facilitate the OAT reaction, an aspect which was discussed by Fields et al.[5] The general preference for nitrogen end-on coordination of nitrous oxide to a metal center has been determined to be a function of π back-bonding.[16, 5] In his review of the use of nitrous oxide as an oxidant, Tolman[16] highlighted that to donate the oxygen atom to an open site on a metal the general consensus is that back-donation of electrons from the metal to the anti-bonding π orbital of nitrous oxide ultimately facilitates the cleavage of the oxygen-nitrogen bond(s). The frontier orbitals of nitrous oxide are shown in Figure A.1 in the Appendix and how the energy of these orbitals and their shape changes with the alteration of the nitrogen-nitrogen-oxygen angle of nitrous oxide; both orbitals in the figure have degenerate partners which reside perpendicular to the them. The 2π orbitals in the figure are doubly occupied and are bonding with respect to the nitrogen atoms and anti-bonding between nitrogen and oxygen while the 3π orbitals are unoccupied and anti-bonding with regards to all atoms in nitrous oxide, this 3π orbital is the aforementioned anti-bonding orbital considered critical to the oxygen transfer reaction.

As π back-bonding is impacted by the ligand field round a metal center, tuning the ligand field not only has the capacity to influence the OAT reaction but also the coordination of N_2O to the metal center. Fields et al.[5] have previously studied the coordination of N_2O to group 8 transition metals and have provided a measure of insight into how the ligand field can influence the coordination mode preference of

N_2O. However, the impact of the ligand field on the oxygen atom transfer reaction itself has not been well well studied, especially for high spin (S=2) iron(II) complexes. When a strong ligand field is employed in an iron(IV)-oxo complex the S=1 spin state tends to be preferred, this is sometimes referred to as generation 1. If instead a weaker ligand field is utilized the S=2 high spin state tends to be favored, this is sometimes referred to as generation 2. This work presents a small database constructed to allow for the study of the use of nitrous oxide as an oxidant for the formation of iron(IV)-oxo species. Ligand environments that are likely to favor high spin (S=2) ground states are heavily represented in the database, thus allowing the study of such cases to be a major focus of this work. Auxiliary structures were utilized to interrogate specific observations from the database to either test or clarify the aspects of the observations. These results are employed to inform design principles for iron(II) centered complexes intended to utilize nitrous oxide as an oxidant.

Computational tools and approaches are employed in this work to establish and investigate a database of iron(II) centered complexes that make use of nitrous oxide as the terminal oxidant for the formation of the corresponding iron(IV)-oxo. These tools are used to pursue structure function relations and/or descriptors for the nitrous oxide coordinated intermediate that have predictive capability with respect to the reaction barrier for the oxygen atom transfer reaction without requiring a transition state search. Predictors like this may prove useful to experimental colleagues when working to design and develop molecular complexes and materials that form iron(IV)-oxo sites utilizing N_2O as the terminal oxidant with lower reaction barriers than previously accomplished.

Chapter 2

Computational Approaches

Density functional theory (DFT) calculations have proven to be a versatile tool that has been successfully employed to computationally investigate a variety of chemical questions. For the present work the DFT level of theory was selected to be used for all computations as it provides reasonable accuracy without the computational cost associated with more accurate approaches such as coupled cluster calculations. Furthermore, as a consequence of the reasonable accuracy and reduced computational cost DFT is useful for conducting transition state searches which can be computationally challenging even with computationally low cost methods as it requires optimizing to a saddle point on the potential energy surface that corresponds to the reaction of interest.

Dr. Kirkland (University of Tennessee alumnus) had previously developed an iron(IV)-oxo database with the molecular geometries of the iron(IV)-oxo species optimized with density functional theory (DFT) using the ORCA 4.2.1[11, 12] quantum chemical program package. With the OPBE[14, 8] density functional having been used since previous work had show that it provides very good accuracy for iron complexes, and the def2-TZVPP[20] basis set and the D3 dispersion correction of Grimme and co-workers[7] with the Becke-Johnson[7, 6] dumping function utilized. Sixty-four of these optimized structures served as the basis for the development of

the database presented in this work and any structures intended to compare to the database directly were initially optimized with the same protocol.

The following set of calculations were performed to construct the database herein reported. For each of the 64 different complexes, the Fe-ON_2 (oxygen end-on) intermediate and the transition state that leads to the dissociation of the O-N bond for the formation of a Fe(IV)-oxo intermediate and N_2 was computed. Each calculation was performed for the singlet, triplet and quintet spin states. DFT geometry optimizations with the M06-L[22] density functional and the def2-TZVPP[20] (Fe), def2-TZVP[20, 19] (C, O, N, F, P), def2-SVP[20, 19] (H) basis sets were performed with using Gaussian 16[26] software package. This functional and these basis sets were selected based on previous literature.[17] For some of the geometry optimizations with the model Fe complexes (structures **1**-**35**) decoordination of H_2O or NH_3 upon N_2O binding was observed when no restraints were applied to structures. For that reason, all atoms except Fe and N_2O were kept frozen during the Fe-ON_2 intermediate and transition state geometry optimizations. Fully relaxed geometries of the reaction intermediate and transition state were computed at the M06-L/def2-TZVPP(Fe)/def2-TZVP(C, O, N)/def2-SVP(H) level for the two molecular complexes with the lowest O-N dissociation reaction barrier (structures **62** and **64**).

The general form for the oxygen atom transfer (OAT) reaction under consideration is given in Figure 2.1. Both the enthalpic reaction barrier ΔH_{RB} and the corresponding Gibbs free energy change were computed for all three spin states (S = 0, 1, 2) using the following equations:

$$\Delta H_{\mathrm{RB}} = H_{\mathrm{TS}} - H_{\mathrm{Fe\text{-}ON_2}} \tag{2.1}$$

where H_{TS} refers to the enthalpy of the OAT transition state for different spin states and $H_{\mathrm{Fe\text{-}ON_2}}$ refers to the enthalpy for the ground spin state of the Fe-ON_2 intermediate.

$$\Delta G_{\mathrm{RB}} = G_{\mathrm{TS}} - G_{\mathrm{Fe\text{-}ON_2}} \tag{2.2}$$

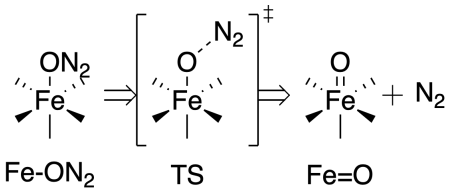

Figure 2.1: General reaction for the oxygen atom transfer reaction utilizing nitrous oxide as the oxidant. The N_2O coordinated intermediate is labeled as Fe-ON_2, the transition state is labeled TS, and the iron-oxo is labeled as Fe=O.

where G_{TS} refers to the Gibbs free energy of the OAT transition state for different spin states and $G_{\mathrm{Fe\text{-}ON_2}}$ refers to the Gibbs free energy for the ground spin state of the Fe-ON_2 intermediate.

All optimizations for ruthenium-based systems utilized the same basic procedure as for the iron based systems together with the SDD[1] pseudo potential for the core electrons of the ruthenium.

Multiwfn 3.8[58] was employed all charge analysis. Specifically, Multiwfn[58] was utilized to determine Mulliken[59], Hirshfeld[60], and Voronoi[61] charges for both the iron(II) center and oxygen atom in the nitrous oxide in nitrous oxide coordinated structures.

Chapter 3

Molecular Database

A database of 64 Fe molecular complexes was generated for the purposes of this study which is an extension of the collection of 55 Fe complexes of Andrikopoulos et al.[2]. The optimized Cartesian coordinates for the nitrous oxide coordinated structures can be found in the attached file **N2O_Structures.txt** while the optimized Cartesian coordinates for the transition state structures can be found in the attached file **TS_Structures.txt**. The 64 molecular complexes are balanced between Fe model complexes and molecular ligand Fe complexes that can accommodate the Fe-oxo intermediate (Figures 3.1 and 3.2), this database overlaps significantly with an iron-oxo database used in the Vogiatzis group and reported on by Jones et al.[62] sans the oxo group. The model complexes are composed by Fe coordinated to primarily H_2O, NH_3, PH_3, small organic components, and/or functionalizations of these. The combination of these two molecular subsets offers a balanced set of different coordination environments with varying ligand field strengths. The H_2O, NH_3, and PH_3 ligands allow for the inclusion of psuedo octahedral and psuedo trigonal bipyramidal model complexes which have systematically varied ligand field strengths (axially and equatorially) which provides the capability to directly assess the impact of ligand field strength on the reaction barrier.

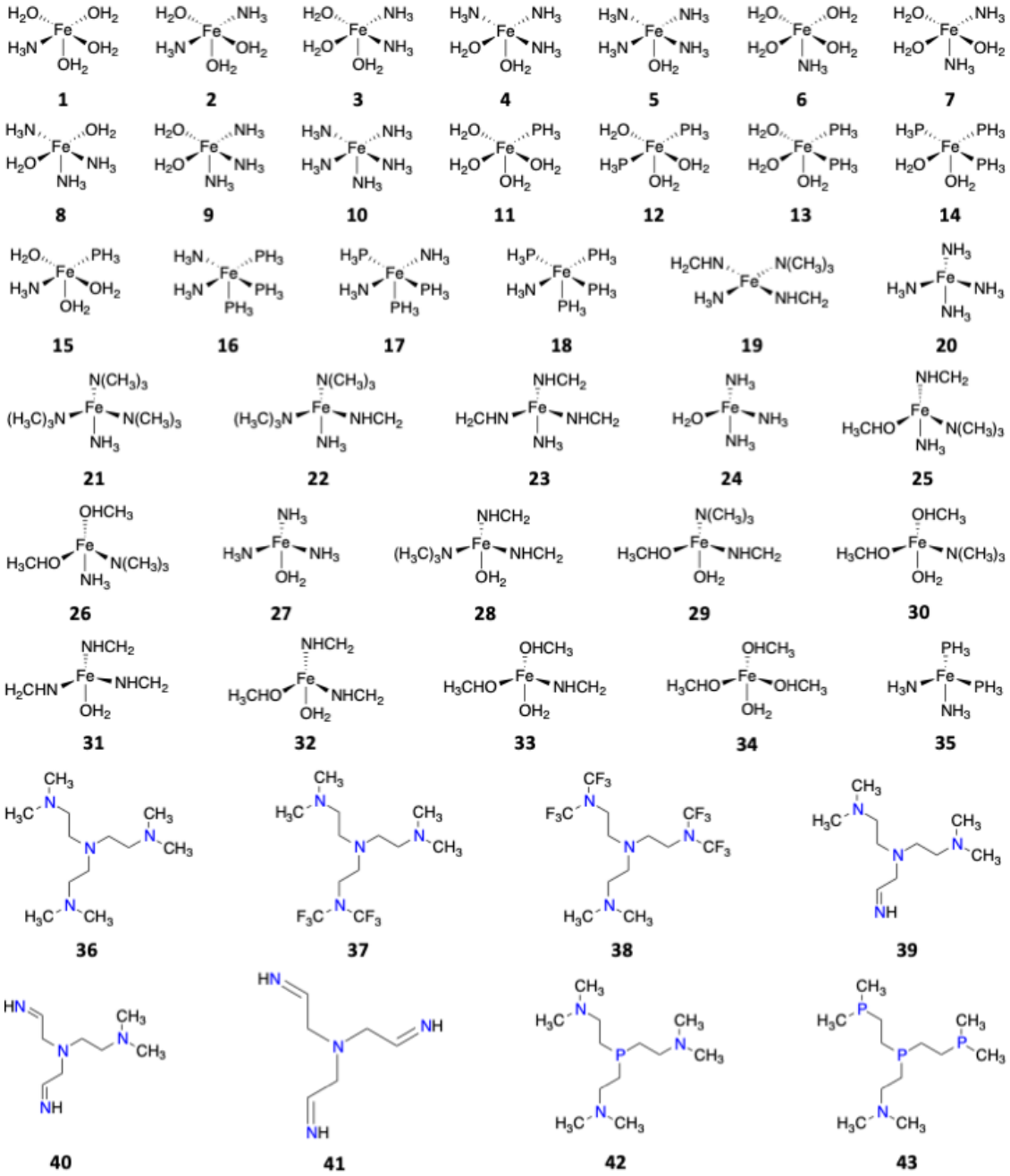

Figure 3.1: Database structures **1** through **43**. For structures **36-43**, atoms coordinated to Fe are shown with blue font.

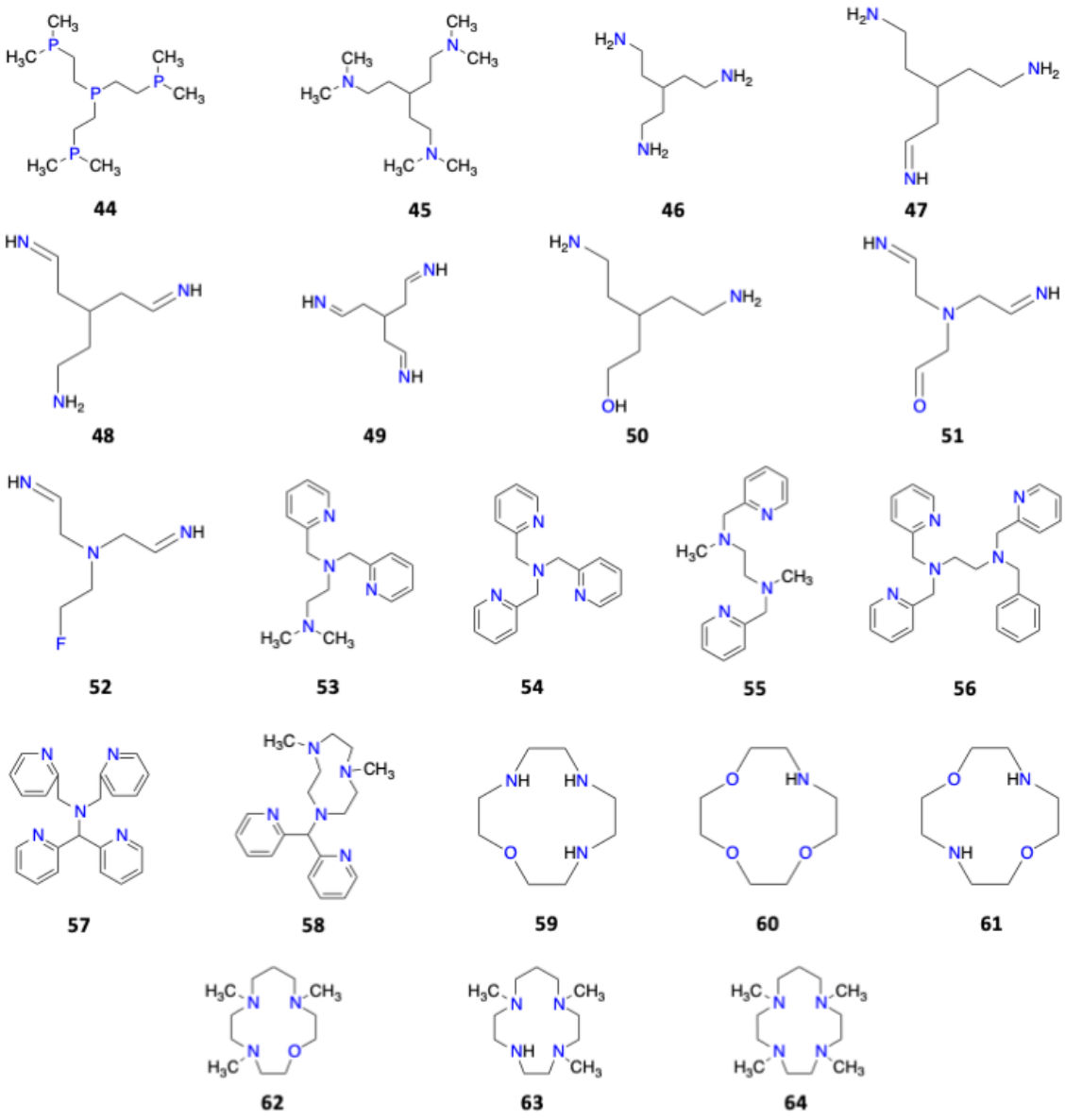

Figure 3.2: Database structures **44** through **64**. Atoms coordinated to Fe are shown with blue font.

The database contains approximately 32% pseudo octahedral complexes, 9% pseudo square pyramidal complexes, and 55% pseudo trigonal-bipyramidal complexes. This variety with respect to the ligand field coordination environment provides a useful database for studying ligand field effects.

For the molecular ligands several previously synthesized ligands and modifications/variants of them were utilized.[23, 24, 25] Structure **36** is a TREN type ligand that is known experimentally[34, 25] and has been used as a ligand for theoretical work as well[33]. A selection of TREN type ligands with differences ranging from substitution changes to the introduction of double bonds and/or change of elements at the four original coordination sites. Structure **54** and related structures represent a scaffold structure known experimentally in iron-oxo chemistry and supramolecular chemistry.[37, 32] Structure **55** utilizes a ligand that is known experimentally [36, 31] to be viable in catalytic intermediates and has been specifically reported as being capable of forming an iron(IV)-oxo species[38] along with variants of the ligand. Structure **57** is also known experimentally for oxidation of C-H bonds via an iron(IV)-oxo species.[36] TATM[23], which is a modification of a ligand used in the study of superoxide reductases[35], and variants of it are represented in the current database (ex. structure **64**, TATM). The inclusion of known ligands along with modifications and variants of those ligands increases the applicability of results obtained from analysis of the currently reported database to experimental work as opposed to being purely theoretical in applicability.

Chapter 4

Analysis

A brief overview and discussion of a single structure is constructive prior to general analysis of the database. For this purpose structure **10** is selected, the ligand field is comprised of the coordinated nitrous oxide and five ammonia ligands resulting in an approximately octahedral ligand field. The mean Fe-NH_3 distance for the equatorial ammonia ligands is 2.04 Angstroms, the Fe-NH_3 distance for the axial ammonia ligand is 2.12 Angstroms, and the Fe-ON_2 distance for the nitrous oxide coordinated antipodal to the axial NH_3 is 2.71 Angstroms. The high spin (S=2) state of structure 10 is the lowest energy state for both the N_2O coordinated intermediate and the transition state for the oxygen atom transfer reaction, this results in an enthalpic reaction barrier of 26.4 kcal/mol and a Gibbs free energy reaction barrier of 28.0 kcal/mol at 298.15 Kelvin.

The 3d-orbital splitting and occupation for the iron(II) center for structure **10** is provided in Figure 4.1. However, this orbital splitting should not be taken as absolute as the 3d orbital occupations suggest the presence of a doubly occupied orbital (the $3d_{xz}$ orbital) with a higher energy than two singly occupied orbitals ($3d_{xy}$ and $3d_{yz}$). This is most probably a consequence of utilizing geometric constraints based on the iron(IV)-oxo pre-optimization that held fixed the coordinates of the ligands other than nitrous oxide during the geometry optimization and transition state search.

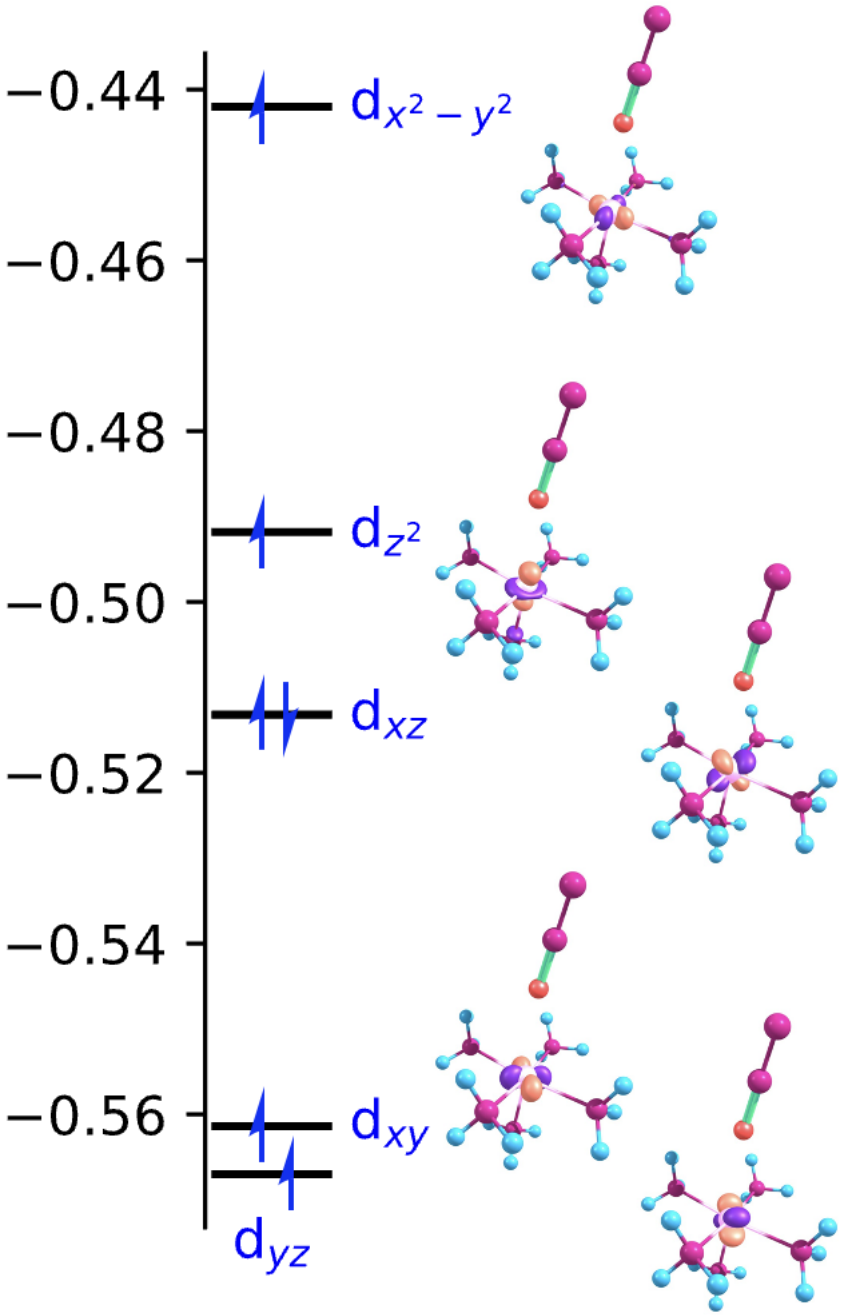

Figure 4.1: Structure 10 Fe(II) center 3d orbital splitting. Orbital energies are given in electronvolts (eV) and isovalue = 0.2 for all orbitals.

Though this reduces the usability of the electronic structure of the 3d orbitals of the iron(II) centers of the studied complexes, the geometric constrains do not invalidate the computed reaction barriers as will be discussed later in this chapter. Furthermore, this does not invalid the use of population analysis methods as those are not impacted by the exact ordering of the electrons but are rather based on the electron populations and different approaches to estimating them.

The enthalpic reaction barrier (ΔH_{RB}) relative to the N_2O coordinated intermediate ground spin state for the structures in the database are summarized in the heat plot in Figure 4.2. The spin multiplicity of the ground state for the N_2O coordinated intermediate and the TS are given as a letter in parenthesis next to the structure number, $(intermediate, TS)$ notation, s = singlet, t = triplet, q = quintet.

The Gibbs free energy reaction barrier (ΔG_{RB}) relative to the N_2O coordinated intermediate ground spin state for the structures in the database are summarized in the heat plot in Figure 4.3. The spin multiplicity of the ground state for the N_2O coordinated intermediate and the TS are given as a letter in parenthesis next to the structure number, $(intermediate, TS)$ notation, s = singlet, t = triplet, q = quintet. Comparison of Figure 4.2 and Figure 4.3 indicates that though the numbers differ between ΔH_{RB} and ΔG_{RB}, which is expected, the inclusion of the entropic term in Gibbs free energy does not change the patterns or trends. Consequently, the analysis of the data will be based on the ΔH_{RB} which is independent of temperature while ΔG_{RB} does varying with temperature; henceforth, unless otherwise specified all made to reaction barriers will be references to the enthalpic reaction barriers.

For convenience the following designations will be utilized: Group 1 for structures **1-18**, the square pyramidal type model ligand fields; Group 2 for structures **20-35**, the trigonal pyramidal type model ligand fields; Group 3 for structures **36-54**, the TREN type and TREN related ligands; Group 4 for structures **56-58**, molecular square pyramidal type ligands; and Group 5 for structures **59-64**, the molecular square planar type ligands.

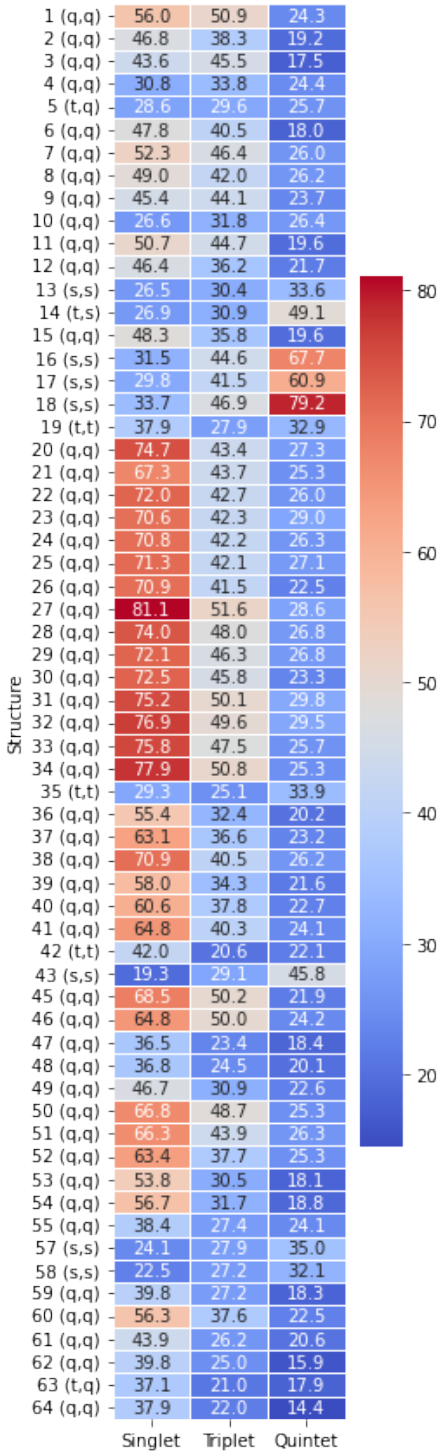

Figure 4.2: Heatmap of enthalpic reaction barriers (ΔH_{RB}) in kcal/mol for the the oxygen atom transfer reaction of the 64 structures. Spin multiplicities are given in parentheses for the N_2O coordinated and TS ground states respectively.

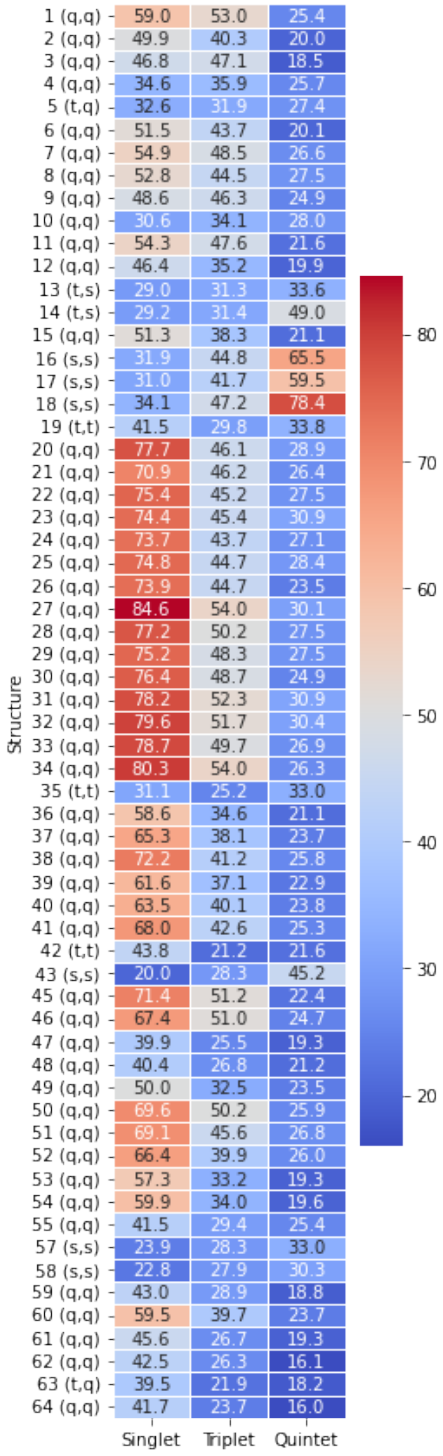

Figure 4.3: Heatmap of Gibbs free energy reaction barriers (ΔG_{RB}) in kcal/mol for the the oxygen atom transfer reaction of the 64 structures. Spin multiplicities are given in parentheses for the N_2O coordinated and TS ground states respectively. Computed at 298.15 Kelvin.

Group 1 has the greatest diversity of ground spin state configurations with 77% of the structures having a high spin (S=2) ground state for both the N_2O coordinated intermediate and the transition state, 11% of the structures having a low spin (S=0) ground state for both the N_2O coordinated intermediate and the transition state, and three structures demonstrate two-state reactivity (**5** with (S=1,S=2), **14** with (S=1,S=0), and **63** with (S=1,S=2) ground states). Group 1 also has the largest range of reaction barriers with reaction barriers ranging from 17.5 kcal/mol to 33.7 kcal/mol a range of 16.2 kcal/mol. Group 2, the other group of model complexes, has reaction barriers which fall within the range of those in Group 1 but does not achieve as low of a reaction barrier with the lowest reaction barrier being only 22.5 kcal/mol. Furthermore, all but one of the complexes in group 2 have a high spin ground state for both the N_2O coordinated intermediate and the transition state with the only exception being **35** which has an intermediate spin (S=1) ground state for both. Proceeding to the groups for molecular ligands, the group 3 complexes similarly fall within the range of reaction barriers for group 1 and also have a majority of high spin ground states with sixteen in total while there is one each of low spin and intermediate spin ground states, the lowest reaction barrier represented in this group is 18.1 kcal/mol. It should be noted that while groups 2 & 3 share the same general coordination geometry, the reaction barriers for group 3 complexes tend to be lower than those for group 2 with the maximum for group 3 being 26.3 kcal/mol as opposed to 29.8 kcal/mol and the minimum for group 3 being 18.1 kcal/mol as opposed to 22.5 kcal/mol for group 2. Moving on the group 4, this is the only group that is not predominated by high spin ground states with all of the structures which converged for all tested spin state having low spin ground states. Group 5 contains the lowest reaction barrier of 14.4 kcal/mol and contains high spin ground states expect for a single structure which demonstrates an intermediate spin N_2O intermediate with a high spin transition state.

In group 1 a pattern is observed via comparing different ligand fields; structures 1 and 2 differ only by a change of a H_2O equatorial ligand to a NH_3 equatorial ligand

resulting in a stronger equatorial ligand field. This increase in equatorial ligand field strength is accompanied by a lower reaction barrier for structure **2**. However, simply increasing the overall ligand field strength is insufficient to achieve the lowest reaction barriers. For example, structure 4 differs from structure 2 by the addition of another equatorial NH_3 in place of an H_2O resulting in a higher reaction barrier than for structure **2**. Further, symmetry of the ligand field can also impact the reaction barrier. Structures **8** and **9** differ by the distribution of the equatorial ligands, in structure **8** the equatorial NH_3 ligands are trans while the equatorial NH_3 ligands in structure **9** are cis resulting in reduced symmetry. Structure **9** has a reaction barrier approximately 2.5 kcal/mol lower than for structure **8**. Asymmetry in the equatorial ligand field is not however indicative of a lower reaction barrier; for instance the opposite pattern is observed in structures **16** and **17**. As such, although symmetry and asymmetry can affect the reaction barrier it is not clearly predictable at this time without computation which scenario will have the lower reaction barrier.

Structures **62** and **64** have the two lowest reaction barriers in the reported database and are both tetradentate ligands with significant similarities, the primary difference being the replacement of the oxygen in structure **62** with a methylated nitrogen in structure **64**. This change results in a stronger equatorial ligand field for structure **64** than for structure **62**. For structures **62** and **64** the ligand field strength is tempered by the organic linkers between the ligating atoms. Structure **64** is the most interesting of these two structures as it has the lowest predicted reaction barrier for the OAT reaction and has a high spin (S = 2) ground state for both the N_2O coordinated structure and the transition state structure. Of note is that structure **64** does not contain an axial ligand which would be opposite to the open coordination site for the coordination and activation of N_2O. Structure **62** has a computed ΔH_{RB} about 1 kcal/mol higher than structure **64**. Like structure **64**, structure **62** has a quintet/quintet ground state combination and lacks an axial ligand to possibly weaken the coordination of N_2O and thereby increase the reaction barrier (*vide infra*).

Full unconstrained optimization was performed for both structures **62** and **64** to compute the associated reaction barriers. The quintet ground state was maintained for both the N_2O coordinated intermediate and transition state structures of structures **62** and **64**. The unconstrained computation of the reaction barriers resulted in a reaction barrier of 18.3 kcal/mol for structure **62** and 16.4 kcal/mol for structure 64 in comparison to the constrained optimization reaction barriers of 15.9 kcal/mol and 14.4 kcal/mol respectively. The differences between the unconstrained and constrained reaction barriers are less than 3 kcal/mol which is within the commonly accepted error of 2-3 kcal/mol accuracy of DFT calculations. This increases the confidence in the other constrained optimization reaction barriers.

Structures **18** and **16** have the highest reaction barriers (33.7 and 31.5 kcal/mol respectively) among all structures present in the database. Both structures share a phosphine axial ligand and at least two phosphine equatorial ligands with structure **18** having three and structure **16** two, the remaining equatorial ligands are ammonia(s). These both represent strong ligand environments, strong enough to increase the reaction barrier rather than lower it, with a strong axial ligand antipodal to the coordinating N_2O. Furthermore, for both of these structures the ground state is the singlet state for both the N_2O coordinated intermediate and the transition state rather than the quintet ground states in the best performing structures (**62** and **64**).

The structures in Figure 4.4 demonstrate some interesting patterns for the more general set of complexes that performed well. In all structures in Figure 4.4 nitrogen is present in the ligand field, which other than phosphorous containing ligands will produce the strongest ligand fields in this structural database. Phosphorous is also represented in structures **15** and **43**. However, comparison of structure **2** and structure **15** (differing by the substitution of an ammonia in structure **2** for a phosphine in structure 15) demonstrates that the increased ligand field strength of phosphine over ammonia has no advantage relative to lowering the reaction barrier. While the best two cases (structures 62 and 64) do not utilize axial ligands, axial ligands are present in these well performing complexes. Also of note is that while a

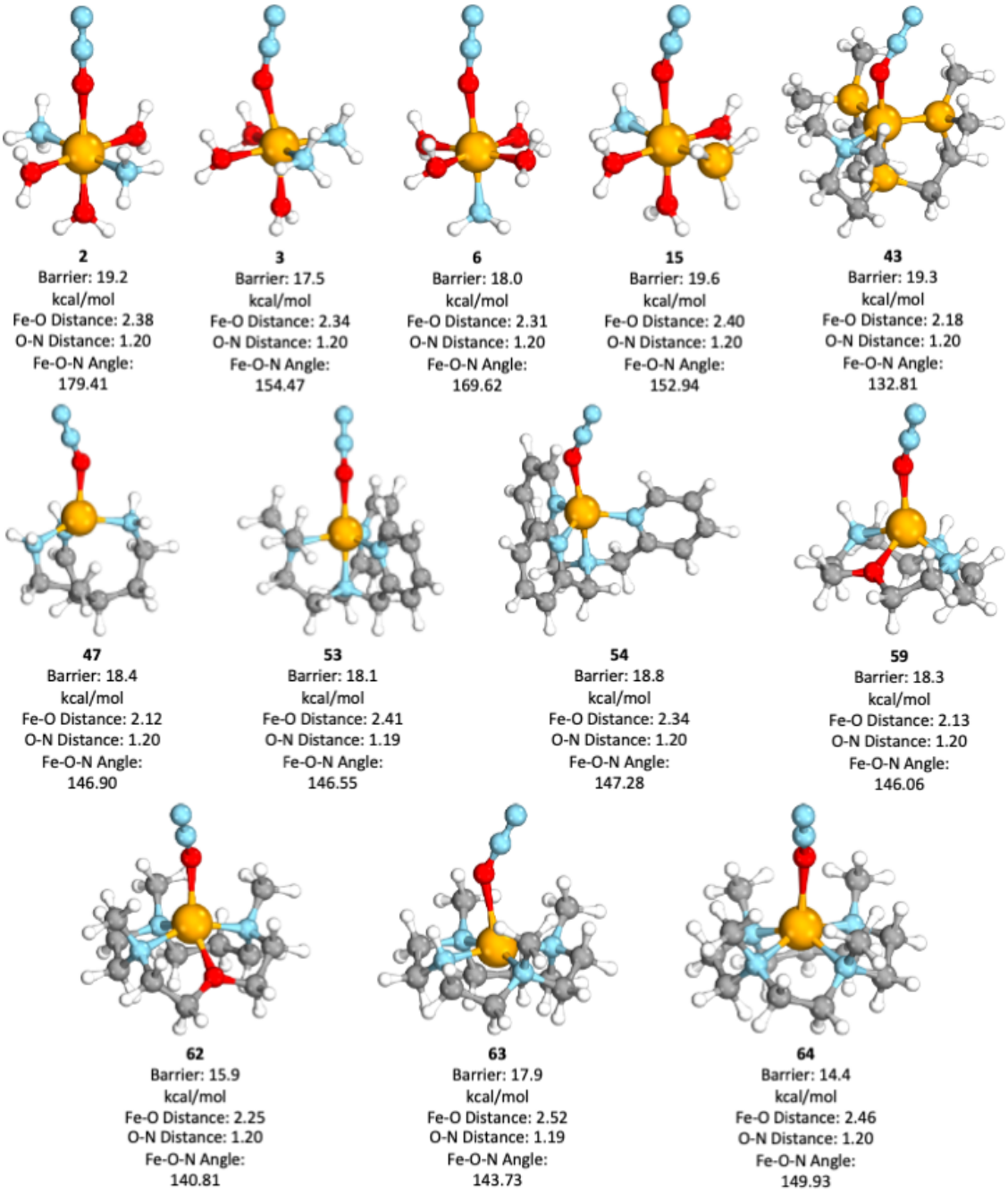

Figure 4.4: Optimized nitrous oxide coordinated structures with important structural parameters and the OAT enthalpic reaction barrier listed for several structures of interest, the best 12 cases.

third of the structures in Figure 4.4 have only three equatorial ligands instead of four, these structures do not go below a reaction barrier of 18 kcal/mol while half of the structures in Figure 4.4 with four equatorial ligands have a reaction barrier of less than 18 kcal/mol. This tends to indicate that the use of four equatorial ligands is preferable to the use of three equatorial ligands though not necessarily fully exclusive. To investigate the impact of axial ligands on the the reaction barrier for the OAT reaction four model systems were constructed being comprised of 4 equatorial H_2O ligands and an axial ligand, an additional system comprised of only 4 equatorial H_2O ligands was also investigated. The four axial ligands chosen were: H_2O, NH_3, PH_3, and CO. These ligands cover a spread of the spectrochemical series and thereby allow a direct assessment of the affect of axial ligands. The lowest OAT reaction barrier was for no axial ligand with the H_2O axial ligand having a 4.0 kcal/mol larger barrier, NH_3 having a 5.4 kcal/mol higher reaction barrier, PH_3 resulting in a 5.4 kcal/mol larger reaction barrier, and the strongest lignad CO producing a 5.8 kcal/mol greater reaction barrier relative to having no axial ligand. The d_{z^2} orbital energies for the no axial ligand structure and the 4 axial ligand structures with N_2O coordinated are plotted against the corresponding reaction barriers in Figure A.2 in the Appendix. The plot demonstrates that for no axial ligand, H_2O, and NH_3 a higher d_{z^2} orbital energy correlates to a higher reaction barrier. CO and PH_3 as axial ligands do not fit this pattern and are also the two strongest axial ligands investigated. This suggests that to minimize the OAT reaction barrier axial ligands should ideally be avoided, and if an axial ligand cannot be avoided then a weaker axial ligand should be selected. It was initially anticipated that either the iron-oxygen distance or the oxygen-nitrogen distance in the nitrous oxide coordinated structures would demonstrate at least a weak correlation to the reaction barrier for the oxygen atom transfer reaction. The shorter the iron-oxygen distance the closer the structure is to the target iron-oxo and the longer the oxygen-nitrogen distance in the nitrous oxide the more activated the N_2O should be. Table A.1 in the Appendix reports the aforementioned distances in Angstroms(Å). Analysis of the oxygen-nitrogen bond distance data reveals that only

two bond distances are observed (1.19 Å and 1.20 Å), this is insufficient variability to produce any significant mathematical correlation. Unlike the oxygen-nitrogen distances the iron-oxygen distances demonstrate significantly more variability. Initial plotting of iron-oxygen distances versus the corresponding reaction barriers for the high spin cases shows no correlation. If the data is subdivided by coordination environment geometry (psuedo square pyramidal, psuedo octahedral, and pseudo trigonal bipyramidal), the psuedo square pyramidal (Figure A.3 in the Appendix) and psuedo octahedral (Figure A.4 in the Appendix) structures both show weak correlations. However, while the psuedo octahedral structures have a correlation in which a shorter iron-oxygen distance correlates to a smaller reaction barrier the psuedo square pyramidal structures have the opposite correlation. Given this disparity, the weakness of the correlations, and the size of the data set neither of these correlations should be considered predictive.

A correlation of significant interest was identified for the psuedo square pyramidal ligand environments with a quintet ground state for both the N_2O coordinated structures (Figure A.5 in the Appendix). This correlation allows the prediction of the reaction barrier for the OAT reaction without having to optimize the transition state structure with reasonable accuracy by utilizing the energy of a single molecular orbital. No similar correlation was found for any of the other ligand environment geometries in the database studied.

To further investigate this apparent correlation, a group of auxiliary structures with psuedo square pyramidal coordination environments was created via modifying structures **62** and **64**. Seven additional high spin (S=2)/quintet ground state structures were identified (Figure A.6 in the Appendix). Incorporation of the HOMO-3 α-orbital energy and enthalpic reaction barrier data from these additional structures is shown in Figure A.7 in the Appendix. While the correlation is weaker than the original correlation, there is still a significant correlation. However, the origin of this correlation has still not been established as it has not been found to correspond to a specific d orbital and therefore requires further investigation.

Three different charge models (Mulliken[59], Hirshfeld[60], and Voronoi[61]) were employed to investigate the possibility of a connection between the charge(s) and the reaction barrier. For this the structures with a nitrous oxide coordinated ground spin state of S=2 were focused on. The least random distributions were the Mulliken charge on the iron center (Figure A.8 in the Appendix) and the Voronoi charge for the oxygen of the coordinated nitrous oxide (Figure A.9 in the Appendix).

A similar breakdown analysis to that employed for the iron-oxygen distance was performed for the Mulliken charges on iron and the Voronoi charges on the oxygen of the nitrous oxide. While the further analysis of the Voronoi charges yielded no significant correlations, further analysis of the Mulliken charges on the iron centers for the high spin cases (Table A.2 in the Appendix) did provide a correlation of interest. Specifically, a strong correlation was observed for the psuedo square pyramidal structures (see Figure A.10 in the Appendix). When the Mulliken charges for the auxiliary psuedo square pyramidal structures previously used to further investigate the HOMO-3 orbital energy correlation are included (with the exception of a negative outlier) the resulting correlation is shown in Figure A.11 in the Appendix. It is notable that the correlation is largely maintained and suggests that a lower Mulliken charge on the iron center will tend to result in a lower reaction barrier for the oxygen atom transfer reaction. This in turn suggests that ligands that are electron donating, thereby decreasing the charge on iron, should be of particular interest when attempting to design such complexes to achieve a low OAT reaction barrier.

Ruthenium is a commonly utilized metal center for catalytic applications and therefore also of interest for comparison to iron. Ruthenium variants of the two best iron center based complexes (structure **62** and structure **64**) constructed and the OAT reaction barriers were computed for comparative analysis with the iron versions. In both cases substitution of ruthenium(II) for iron(II) resulted in a higher enthalpic reaction barrier for the OAT reaction. This suggests that although iron(II) and ruthenium(II) are both d^6 group 8 metals different ligand environments are likely needed to minimize the OAT reaction barrier for ruthenium complexes.

Since MOFs are comprised of metal nodes surrounded and connected by organic linkers, the tempering of the ligand field strength evidently needed can conceivably be provided by tuning the organic linkers in MOFs. A localized nitrogen rich ligand field around each iron(II) node tempered by tuned organic linkers may provide a viable MOF catalyst for the OAT reaction and activation of N_2O. Study of potential and known MOF structures informed by the previously discussed patterns will be required to achieve organic linkers sufficient to both support the synthesis of crystalline MOF structures while also appropriately tempering the ligand field strength. Achieving the equivalent of no axial ligand in a MOF may be significantly difficult however.

Chapter 5

Conclusion

This work reported a database of structures containing both model and molecular for the study of the oxygen atom transfer (OAT) reaction barrier for Fe(II) systems with nitrous oxide fulfilling the role of oxygen source/oxidant. Further, this work explored patterns present in the database as well as reports the results of assessing the current database for specific design principles and/or correlations between specific electronic structure properties and the OAT reaction barrier. The patterns, principles, and correlations demonstrated and derived from the resultant data from the entire database presented here along with the auxiliary psuedo square pyramidal cases can guide exploration of not only the molecular chemical space for catalyst candidates but also potentially other chemical spaces such as the Metal Organic Framework (MOF) chemical space.

An intermediate strength equatorial ligand field, roughly in the middle of the traditional spectrochemical series, is recommended as the starting point for catalyst design in this context. Specifically, a square or psuedo square planar equatorial ligand field is advised based on the results presented herein. If axial components (other than the coordinating N_2O) to the metal's ligand field cannot be avoided then careful selection of these axial components or interactions is to be as weak as possible is recommended in order to minimize the OAT reaction barrier.

Two distinct correlations to the OAT reaction barrier were identified for the psuedo square pyramidal nitrous oxide coordinated structures: the HOMO-3 α molecular orbital energy (Figure A.7 in the Appendix) and the Mulliken charge on the iron center of the N_2O coordinated structures (Figure A.11 in the Appendix). Both of these correlations demonstrate strong correlations and therefore may indeed prove to be viable predictive metrics in the experiment design and synthesis of such iron(IV)-oxo catalytic species. It should be noted though that the identification of a clear causal relationship underpinning the HOMO-3 orbital correlation has so far proven elusive and warrants further investigation and study.

Based on the unexpected under-performance of the utilized charge models and the limited understanding of the correlation involving the HOMO-3 orbitals (which only applies to a limited subset of structures), the development of novel metrics and/or descriptors is a promising direction for furthering this line of research. Especially with respect to metrics and descriptors that are more broadly applicable across different coordination geometries and configurations. Furthermore, this database and auxiliary structures can be used to assist the development of these metrics/descriptors. Such metrics and descriptors are likely to be applicable not only to iron and nitrous oxide system but also to a variety of other chemical systems.

Bibliography

[1] Andrae, D., Häußermann, U., Dolg, M., Stoll, H. & Preuß, H. Energy-adjusted ab initio pseudopotentials for the second and third row transition elements. *Theoretica Chimica Acta*. **77**, 123-141 (1990), https://doi.org/10.1007/BF01114537 9

[2] Andrikopoulos, P., Michel, C., Chouzier, S. & Sautet, P. In Silico Screening of Iron-Oxo Catalysts for CH Bond Cleavage. *ACS Catalysis*. **5**, 2490-2499 (2015) 10

[3] Barona, M., Ahn, S., Morris, W., Hoover, W., Notestein, J., Farha, O. & Snurr, R. Computational Predictions and Experimental Validation of Alkane Oxidative Dehydrogenation by Fe2M MOF Nodes. *ACS Catalysis*. **10**, 1460-1469 (2020), https://doi.org/10.1021/acscatal.9b03932 3

[4] Bols, M., Snyder, B., Rhoda, H., Cnudde, P., Fayad, G., Schoonheydt, R., Van Speybroeck, V., Solomon, E. & Sels, B. Coordination and activation of nitrous oxide by iron zeolites. *Nature Catalysis*. **4**, 332-340 (2021), https://doi.org/10.1038/s41929-021-00602-4 2, 4

[5] Fields, K., Barngrover, B. & Gary, J. Computational Investigation of the Preferred Binding Modes of N2O in Group 8 Metal Complexes. *Inorganic Chemistry*. (2020), https://doi.org/10.1021/acs.inorgchem.0c02903 4

[6] Grimme, S., Antony, J., Ehrlich, S. & Krieg, H. A consistent and accurate ab initio parametrization of density functional dispersion correction (DFT-D) for

the 94 elements H-Pu. *The Journal Of Chemical Physics.* **132**, 154104 (2010), https://doi.org/10.1063/1.3382344 6

[7] Grimme, S., Ehrlich, S. & Goerigk, L. Effect of the damping function in dispersion corrected density functional theory. *Journal Of Computational Chemistry.* **32**, 1456-1465 (2011), https://doi.org/10.1002/jcc.21759 6

[8] Hoe, W., Cohen, A. & Handy, N. Assessment of a new local exchange functional OPTX. *Chemical Physics Letters.* **341**, 319-328 (2001), https://www.sciencedirect.com/science/article/pii/S0009261401005814 6

[9] McCarver, G., Rajeshkumar, T. & Vogiatzis, K. Computational catalysis for metal-organic frameworks: An overview. *Coordination Chemistry Reviews.* **436** pp. 213777 (2021), https://www.sciencedirect.com/science/article/pii/S0010854521000114 2, 4

[10] Nazaries, L., Murrell, J., Millard, P., Baggs, L. & Singh, B. Methane, microbes and models: fundamental understanding of the soil methane cycle for future predictions. *Environmental Microbiology.* **15**, 2395-2417 (2013), https://doi.org/10.1111/1462-2920.12149 1

[11] Neese, F. The ORCA program system. *WIREs Computational Molecular Science.* **2**, 73-78 (2012), https://doi.org/10.1002/wcms.81 6

[12] Neese, F. Software update: the ORCA program system, version 4.0. *WIREs Computational Molecular Science.* **8**, e1327 (2018), https://doi.org/10.1002/wcms.1327 6

[13] Pannov, G., Sobolev, V. & Kharitonov, A. The role of iron in N2O decomposition on ZSM-5 zeolite and reactivity of the surface oxygen formed. *Journal Of Molecular Catalysis.* **61**, 85-97 (1990), https://www.sciencedirect.com/science/article/pii/030451029085197P 1

[14] Perdew, J., Burke, K. & Ernzerhof, M. Generalized Gradient Approximation Made Simple. *Physical Review Letters*. **77**, 3865-3868 (1996), https://link.aps.org/doi/10.1103/PhysRevLett.77.3865 6

[15] Snyder, B., Vanelderen, P., Bols, M., Hallaert, S., Böttger, L., Ungur, L., Pierloot, K., Schoonheydt, R., Sels, B. & Solomon, E. The active site of low-temperature methane hydroxylation in iron-containing zeolites. *Nature*. **536**, 317-321 (2016), https://doi.org/10.1038/nature19059 1

[16] Tolman, W. Binding and activation of N2O at transition-metal centers: recent mechanistic insights. *Angew Chem Int Ed Engl*. **49**, 1018-24 (2010), https://www.ncbi.nlm.nih.gov/pubmed/20058284 4

[17] Verma, P., Vogiatzis, K., Planas, N., Borycz, J., Xiao, D., Long, J., Gagliardi, L. & Truhlar, D. Mechanism of Oxidation of Ethane to Ethanol at Iron(IV)–Oxo Sites in Magnesium-Diluted Fe2(dobdc). *Journal Of The American Chemical Society*. **137**, 5770-5781 (2015), https://doi.org/10.1021/jacs.5b00382 2, 4, 7

[18] Wang, V., Maji, S., Chen, P., Lee, H., Yu, S. & Chan, S. Alkane Oxidation: Methane Monooxygenases, Related Enzymes, and Their Biomimetics. *Chemical Reviews*. **117**, 8574-8621 (2017), https://doi.org/10.1021/acs.chemrev.6b00624

[19] Weigend, F. Accurate Coulomb-fitting basis sets for H to Rn. *Physical Chemistry Chemical Physics*. **8**, 1057-1065 (2006), http://dx.doi.org/10.1039/B515623H 7

[20] Weigend, F. & Ahlrichs, R. Balanced basis sets of split valence, triple zeta valence and quadruple zeta valence quality for H to Rn: Design and assessment of accuracy. *Physical Chemistry Chemical Physics*. **7**, 3297-3305 (2005), http://dx.doi.org/10.1039/B508541A 6, 7

[21] Xiao, D., Bloch, E., Mason, J., Queen, W., Hudson, M., Planas, N., Borycz, J., Dzubak, A., Verma, P., Lee, K., Bonino, F., Crocella, V., Yano, J., Bordiga, S., Truhlar, D., Gagliardi, L., Brown, C. & Long, J. Oxidation of ethane to ethanol by

N2O in a metal-organic framework with coordinatively unsaturated iron(II) sites. *Nat Chem.* **6**, 590-5 (2014), https://www.ncbi.nlm.nih.gov/pubmed/24950328 2

[22] Zhao, Y. & Truhlar, D. A new local density functional for main-group thermochemistry, transition metal bonding, thermochemical kinetics, and noncovalent interactions. *The Journal Of Chemical Physics.* **125**, 194101 (2006), https://doi.org/10.1063/1.2370993 7

[23] Nam, W. High-Valent Iron(IV)–Oxo Complexes of Heme and Non-Heme Ligands in Oxygenation Reactions. *Accounts Of Chemical Research.* **40**, 522-531 (2007), https://doi.org/10.1021/ar700027f 13

[24] Oloo, W. & Que, L. Bioinspired Nonheme Iron Catalysts for C–H and C=C Bond Oxidation: Insights into the Nature of the Metal-Based Oxidants. *Accounts Of Chemical Research.* **48**, 2612-2621 (2015), https://doi.org/10.1021/acs.accounts.5b00053 13

[25] Usharani, D., Janardanan, D., Li, C. & Shaik, S. A Theory for Bioinorganic Chemical Reactivity of Oxometal Complexes and Analogous Oxidants: The Exchange and Orbital-Selection Rules. *Accounts Of Chemical Research.* **46**, 471-482 (2013), https://doi.org/10.1021/ar300204y 13

[26] Frisch, M., Trucks, G., Schlegel, H., Scuseria, G., Robb, M., Cheeseman, J., Scalmani, G., Barone, V., Petersson, G., Nakatsuji, H., Li, X., Caricato, M., Marenich, A., Bloino, J., Janesko, B., Gomperts, R., Mennucci, B., Hratchian, H., Ortiz, J., Izmaylov, A., Sonnenberg, J., Williams-Young, D., Ding, F., Lipparini, F., Egidi, F., Goings, J., Peng, B., Petrone, A., Henderson, T., Ranasinghe, D., Zakrzewski, V., Gao, J., Rega, N., Zheng, G., Liang, W., Hada, M., Ehara, M., Toyota, K., Fukuda, R., Hasegawa, J., Ishida, M., Nakajima, T., Honda, Y., Kitao, O., Nakai, H., Vreven, T., Throssell, K., Montgomery, J., Peralta, J., Ogliaro, F., Bearpark, M., Heyd, J., Brothers, E., Kudin, K., Staroverov, V., Keith, T., Kobayashi, R., Normand, J., Raghavachari, K., Rendell, A., Burant,

J., Iyengar, S., Tomasi, J., Cossi, M., Millam, J., Klene, M., Adamo, C., Cammi, R., Ochterski, J., Martin, R., Morokuma, K., Farkas, O., Foresman, J. & Fox, D. Gaussian˜16 Revision C.01. (2016), Gaussian Inc. Wallingford CT 7

[27] Kazaryan, A. & Baerends, E. Ligand Field Effects and the High Spin-High Reactivity Correlation in the H Abstraction by Non-Heme Iron(IV)-Oxo Complexes: A DFT Frontier Orbital Perspective. *ACS Catalysis*. **5**, 1475-1488 (2015), https://doi.org/10.1021/cs501721y 3

[28] Liao, P., Getman, R. & Snurr, R. Optimizing Open Iron Sites in Metal–Organic Frameworks for Ethane Oxidation: A First-Principles Study. *ACS Applied Materials & Interfaces*. **9**, 33484-33492 (2017), https://doi.org/10.1021/acsami.7b02195 3

[29] Solomon, E., Light, K., Liu, L., Srnec, M. & Wong, S. Geometric and Electronic Structure Contributions to Function in Non-heme Iron Enzymes. *Accounts Of Chemical Research*. **46**, 2725-2739 (2013), https://doi.org/10.1021/ar400149m 3

[30] Vogiatzis, K., Haldoupis, E., Xiao, D., Long, J., Siepmann, J. & Gagliardi, L. Accelerated Computational Analysis of Metal–Organic Frameworks for Oxidation Catalysis. *The Journal Of Physical Chemistry C*. **120**, 18707-18712 (2016), https://doi.org/10.1021/acs.jpcc.6b07115 2

[31] Balland, V., Charlot, M., Banse, F., Girerd, J., Mattioli, T., Bill, E., Bartoli, J., Battioni, P. & Mansuy, D. Spectroscopic Characterization of an FeIV Intermediate Generated by Reaction of XO- (X = Cl, Br) with an FeII Complex Bearing a Pentadentate Non-Porphyrinic Ligand - Hydroxylation and Epoxidation Activity. *European Journal Of Inorganic Chemistry*. **2004**, 301-308 (2004), https://doi.org/10.1002/ejic.200300287 13

[32] Bravin, C., Badetti, E., Licini, G. & Zonta, C. Tris(2-pyridylmethyl)amines as emerging scaffold in supramolecular

chemistry. *Coordination Chemistry Reviews.* **427** pp. 213558 (2021), https://www.sciencedirect.com/science/article/pii/S0010854520304872 13

[33] Cho, K., Shaik, S. & Nam, W. Theoretical predictions of a highly reactive non-heme Fe(iv)=O complex with a high-spin ground state. *Chemical Communications.* **46**, 4511-4513 (2010), http://dx.doi.org/10.1039/C0CC00292E 13

[34] Cousins, D., Davidson, M., Frankis, C., García-Vivó, D. & Mahon, M. Tris(2-dimethylaminoethyl)amine: a simple new tripodal polyamine ligand for Group 1 metals. *Dalton Transactions.* **39**, 8278-8280 (2010), http://dx.doi.org/10.1039/C0DT00567C 13

[35] Fiedler, A., Halfen, H., Halfen, J. & Brunold, T. Synthesis, Structure Determination, and Spectroscopic/Computational Characterization of a Series of Fe(II)-Thiolate Model Complexes: Implications for Fe-S Bonding in Superoxide Reductases. *Journal Of The American Chemical Society.* **127**, 1675-1689 (2005), https://doi.org/10.1021/ja046939s 13

[36] Kaizer, J., Klinker, E., Oh, N., Rohde, J., Song, W., Stubna, A., Kim, J., Münck, E., Nam, W. & Que, L. Nonheme FeIVO Complexes That Can Oxidize the C-H Bonds of Cyclohexane at Room Temperature. *Journal Of The American Chemical Society.* **126**, 472-473 (2004), https://doi.org/10.1021/ja037288n 13

[37] Lim Mi, H., Rohde, J., Stubna, A., Bukowski Michael, R., Costas, M., Ho Raymond, Y., Münck, E., Nam, W. & Que, L. An FeIVO complex of a tetradentate tripodal nonheme ligand. *Proceedings Of The National Academy Of Sciences.* **100**, 3665-3670 (2003), https://doi.org/10.1073/pnas.0636830100 13

[38] Martinho, M., Banse, F., Bartoli, J., Mattioli, T., Battioni, P., Horner, O., Bourcier, S. & Girerd, J. New Example of a Non-Heme Mononuclear Iron(IV)

Oxo Complex. Spectroscopic Data and Oxidation Activity. *Inorganic Chemistry*. **44**, 9592-9596 (2005), https://doi.org/10.1021/ic051213y 13

[39] Chung, Y., Camp, J., Haranczyk, M., Sikora, B., Bury, W., Krungleviciute, V., Yildirim, T., Farha, O., Sholl, D. & Snurr, R. Computation-Ready, Experimental Metal–Organic Frameworks: A Tool To Enable High-Throughput Screening of Nanoporous Crystals. *Chemistry Of Materials*. **26**, 6185-6192 (2014,10), https://doi.org/10.1021/cm502594j 3

[40] Chung, Y., Haldoupis, E., Bucior, B., Haranczyk, M., Lee, S., Zhang, H., Vogiatzis, K., Milisavljevic, M., Ling, S., Camp, J., Slater, B., Siepmann, J., Sholl, D. & Snurr, R. Advances, Updates, and Analytics for the Computation-Ready, Experimental Metal–Organic Framework Database: CoRE MOF 2019. *Journal Of Chemical & Engineering Data*. **64**, 5985-5998 (2019,11), https://doi.org/10.1021/acs.jced.9b00835 3

[41] Rosen, A., Notestein, J. & Snurr, R. Identifying promising metal–organic frameworks for heterogeneous catalysis via high-throughput periodic density functional theory. *Journal Of Computational Chemistry*. **40**, 1305-1318 (2019,2), https://doi.org/10.1002/jcc.25787 3

[42] Rosen, A., Notestein, J. & Snurr, R. Structure–Activity Relationships That Identify Metal–Organic Framework Catalysts for Methane Activation. *ACS Catalysis*. **9**, 3576-3587 (2019,3), https://doi.org/10.1021/acscatal.8b05178 3

[43] Rosen, A., Notestein, J. & Snurr, R. Realizing the data-driven, computational discovery of metal-organic framework catalysts. *Current Opinion In Chemical Engineering*. **35** pp. 100760 (2022,3), https://doi.org/10.1016/j.coche.2021.100760 3

[44] Gani, T. & Kulik, H. Understanding and Breaking Scaling Relations in Single-Site Catalysis: Methane to Methanol Conversion by Fe^{IV}=O. *ACS Catalysis.* **8**, 975-986 (2018,1), https://doi.org/10.1021/acscatal.7b03597 3

[45] Nandy, A., Zhu, J., Janet, J., Duan, C., Getman, R. & Kulik, H. Machine Learning Accelerates the Discovery of Design Rules and Exceptions in Stable Metal–Oxo Intermediate Formation. *ACS Catalysis.* **9**, 8243-8255 (2019,7), https://doi.org/10.1021/acscatal.9b02165 3

[46] Nandy, A., Duan, C., Goffinet, C. & Kulik, H. New Strategies for Direct Methane-to-Methanol Conversion from Active Learning Exploration of 16 Million Catalysts. *JACS Au.* **2**, 1200-1213 (2022,4), https://doi.org/10.1021/jacsau.2c00176 3

[47] Delahay, G., Mauvezin, M., Coq, B. & Kieger, S. Selective Catalytic Reduction of Nitrous Oxide by Ammonia on Iron Zeolite Beta Catalysts in an Oxygen Rich Atmosphere: Effect of Iron Contents. *Journal Of Catalysis.* **202**, 156-162 (2001), https://www.sciencedirect.com/science/article/pii/S0021951701932798 2

[48] Dubkov, K., Ovanesyan, N., Shteinman, A., Starokon, E. & Panov, G. Evolution of Iron States and Formation of α-Sites upon Activation of FeZSM-5 Zeolites. *Journal Of Catalysis.* **207**, 341-352 (2002), https://www.sciencedirect.com/science/article/pii/S0021951702935529 2

[49] Göltl, F., Michel, C., Andrikopoulos, P., Love, A., Hafner, J., Hermans, I. & Sautet, P. Computationally Exploring Confinement Effects in the Methane-to-Methanol Conversion Over Iron-Oxo Centers in Zeolites. *ACS Catalysis.* **6**, 8404-8409 (2016), https://doi.org/10.1021/acscatal.6b02640 2

[50] Guzmán-Vargas, A., Delahay, G. & Coq, B. Catalytic decomposition of N2O and catalytic reduction of N2O and N2O + NO by NH3 in the presence of

O2 over Fe-zeolite. *Applied Catalysis B: Environmental.* **42**, 369-379 (2003), https://www.sciencedirect.com/science/article/pii/S0926337302002680 2

[51] Jabłońska, M., Delahay, G., Kruczała, K., Błachowski, A., Tarach, K., Brylewska, K., Petitto, C. & Góra-Marek, K. Standard and Fast Selective Catalytic Reduction of NO with NH3 on Zeolites Fe-BEA. *The Journal Of Physical Chemistry C.* **120**, 16831-16842 (2016), https://doi.org/10.1021/acs.jpcc.6b05692 2

[52] Øygarden, A. & Pérez-Ramírez, J. Activity of commercial zeolites with iron impurities in direct N2O decomposition. *Applied Catalysis B: Environmental.* **65**, 163-167 (2006), https://www.sciencedirect.com/science/article/pii/S0926337306000804 2

[53] Rosa, A., Ricciardi, G. & Baerends, E. Is [FeO]2+ the Active Center Also in Iron Containing Zeolites? A Density Functional Theory Study of Methane Hydroxylation Catalysis by Fe-ZSM-5 Zeolite. *Inorganic Chemistry.* **49**, 3866-3880 (2010), https://doi.org/10.1021/ic1000073 2

[54] Yoshizawa, K., Yumura, T., Shiota, Y. & Yamabe, T. Formation of an Iron-Oxo Species upon Decomposition of Dinitrogen Oxide on a Model of Fe-ZSM-5 Zeolite. *Bulletin Of The Chemical Society Of Japan.* **73**, 29-36 (2000), https://doi.org/10.1246/bcsj.73.29 2

[55] Zhilinskaya, E., Delahay, G., Mauvezin, M., Coq, B. & Aboukaïs, A. EPR Investigation of Fe-Exchanged Beta-Zeolites. *Langmuir.* **19**, 3596-3602 (2003), https://doi.org/10.1021/la026137f 2

[56] Hohenberger, J., Ray, K. & Meyer, K. The biology and chemistry of high-valent iron–oxo and iron–nitrido complexes. *Nature Communications.* **3**, 720 (2012), https://doi.org/10.1038/ncomms1718 4

[57] Kal, S., Xu, S. & Que Jr, L. Bio-inspired Nonheme Iron Oxidation Catalysis: Involvement of Oxoiron(V) Oxidants in Cleaving Strong C-H Bonds. *Angewandte Chemie International Edition*. **59**, 7332-7349 (2020), https://doi.org/10.1002/anie.201906551 4

[58] Lu, T. & Chen, F. Multiwfn: A multifunctional wavefunction analyzer. *Journal Of Computational Chemistry*. **33**, 580-592 (2012), https://onlinelibrary.wiley.com/doi/abs/10.1002/jcc.22885 9

[59] Mulliken, R. Electronic Population Analysis on LCAO–MO Molecular Wave Functions. I. *The Journal Of Chemical Physics*. **23**, 1833-1840 (1955), 9, 25

[60] Hirshfeld, F. Bonded-atom fragments for describing molecular charge densities. *Theoretica Chimica Acta*. **44**, 129-138 (1977), https://doi.org/10.1007/BF00549096 9, 25

[61] Fonseca Guerra, C., Handgraaf, J., Baerends, E. & Bickelhaupt, F. Voronoi deformation density (VDD) charges: Assessment of the Mulliken, Bader, Hirshfeld, Weinhold, and VDD methods for charge analysis. *Journal Of Computational Chemistry*. **25**, 189-210 (2004), https://onlinelibrary.wiley.com/doi/abs/10.1002/jcc.10351 9, 25

[62] Jones, G., Smith, B., Kirkland, J. & Vogiatzis, K. Data-driven ligand field exploration of Fe(iv)–oxo sites for C–H activation. *Inorg. Chem. Front.*. **10**, 1062-1075 (2023), http://dx.doi.org/10.1039/D2QI01961B 10

Appendix

The appendix contains figures and tables that were not directly placed in the relevant chapter(s) of this text.

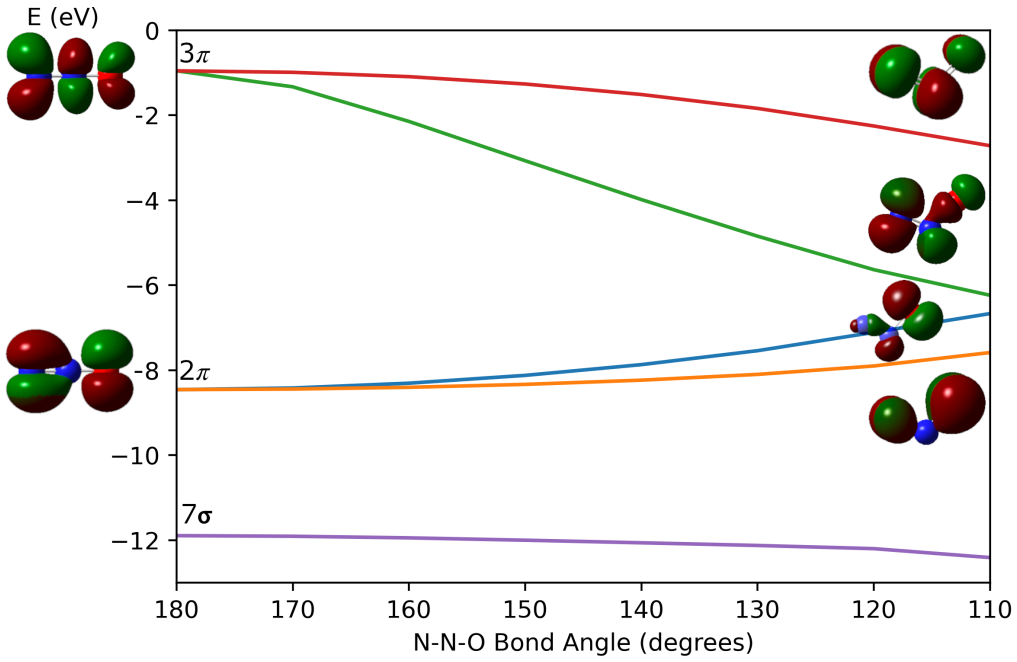

Figure A.1: N_2O frontier orbitals energy and shape with changing N-N-O angle.

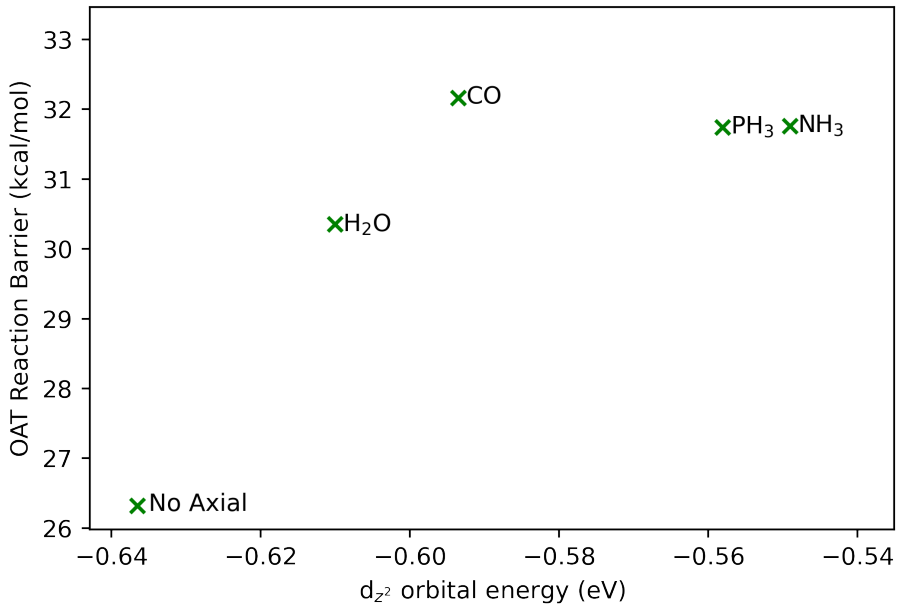

Figure A.2: OAT reaction barriers (RB) vs d_{z^2} orbital energies of N_2O coordinated structures from axial ligand test series.

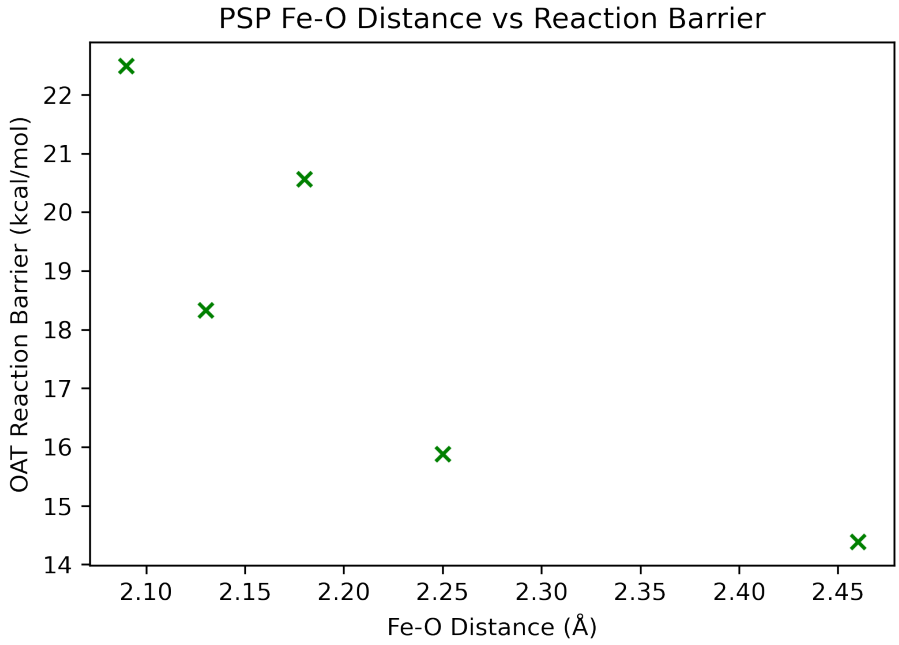

Figure A.3: Fe-O distance vs reaction barrier of N_2O coordinated psuedo square pyramidal (PSP) structures. $R^2 = 0.7297$

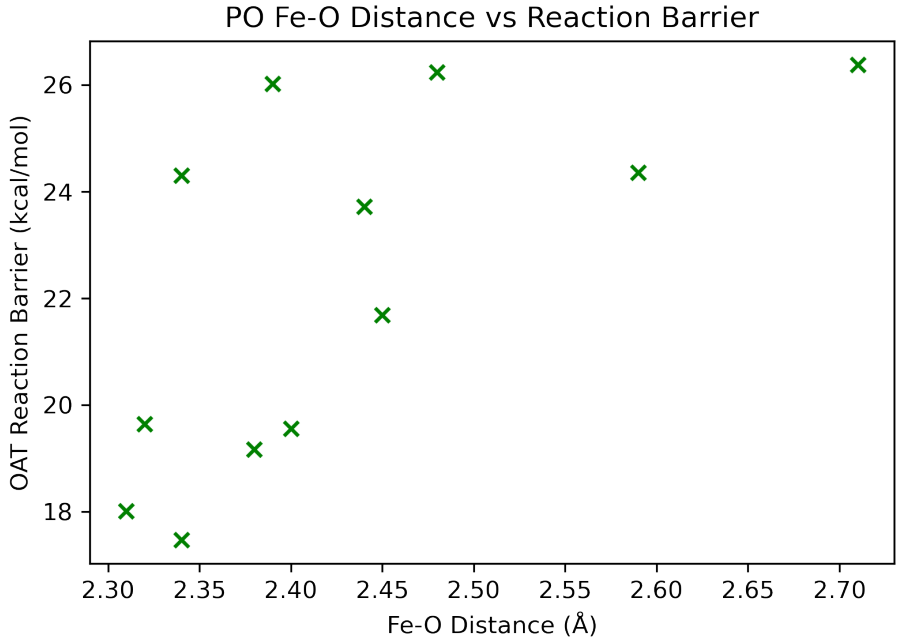

Figure A.4: Fe-O distance vs reaction barrier of N_2O coordinated psuedo octahedral (PO) structures. $R^2 = 0.4197$

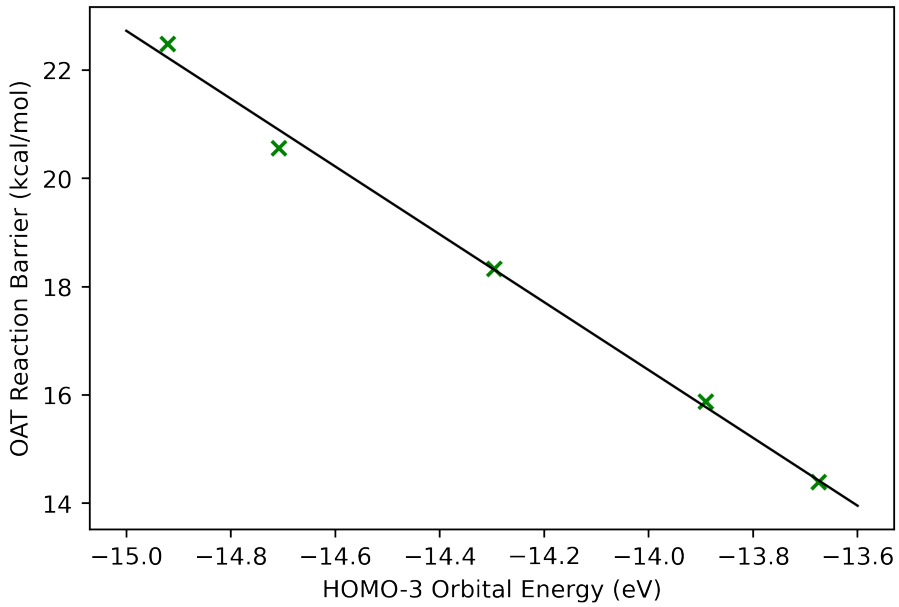

Figure A.5: Correlation between OAT reaction barrier (RB) and HOMO-3 α-orbital energy (OE) of N_2O coordinated psuedo square pyramidal structures. RB = -6.27(OE)-71.29 with $R^2 = 0.9956$

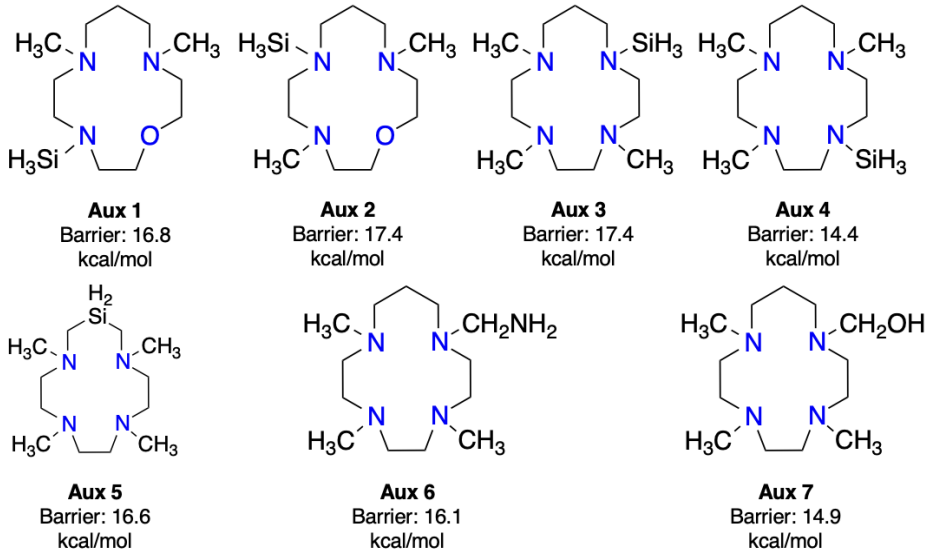

Figure A.6: Auxiliary high spin structures. Enthalpic reaction barriers for the oxygen atom transfer reaction for nitrous oxide are included for each structure.

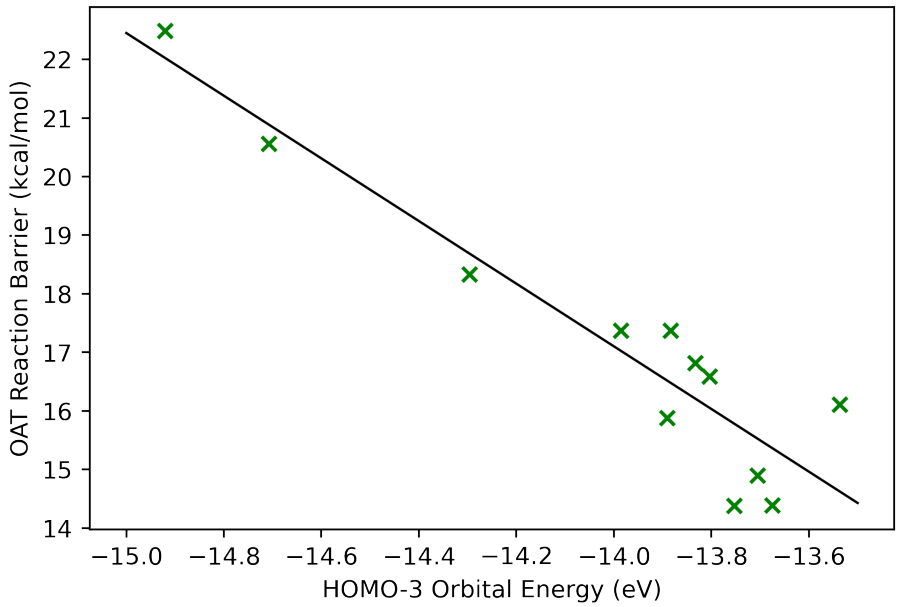

Figure A.7: Correlation between OAT reaction barrier (RB) and HOMO-3 α-orbital energy (OE) of N_2O coordinated psuedo square pyramidal structures including auxiliary structures. RB = -5.35(OE)-57.79 with R^2 = 0.8782

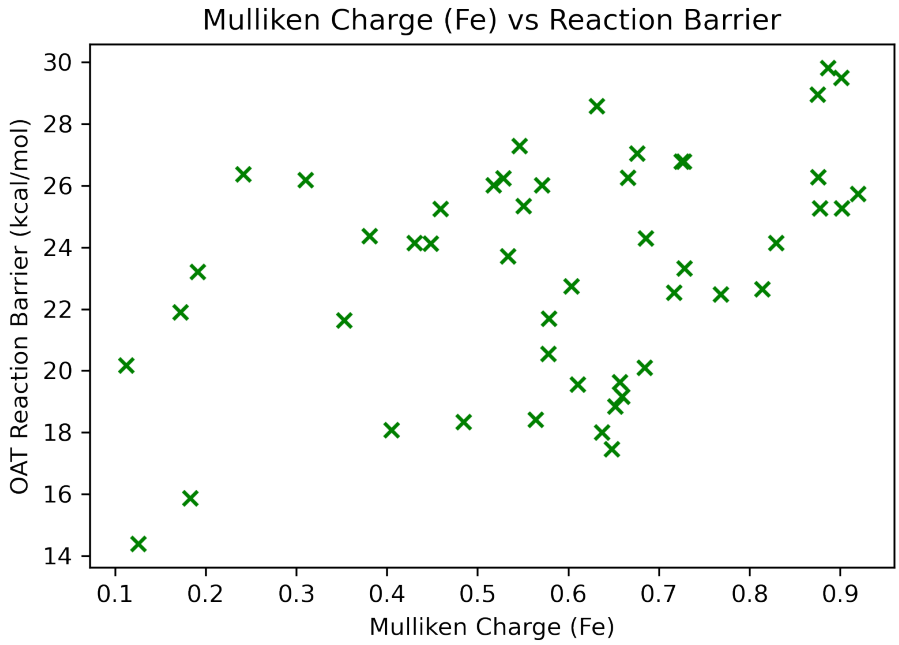

Figure A.8: Mulliken charge of iron vs reaction barriers for the S=2 N_2O coordinated structures.

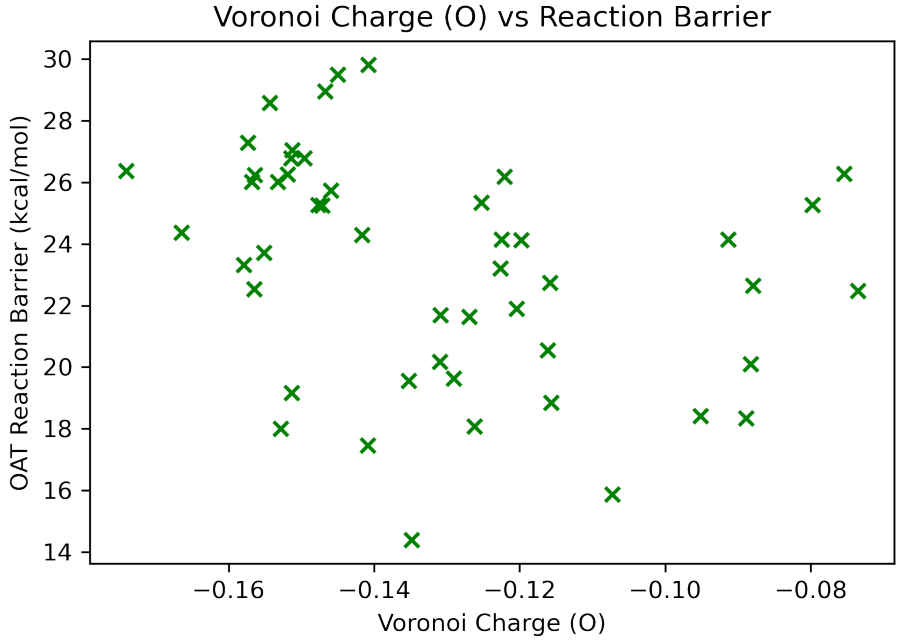

Figure A.9: Voronoi charge of iron vs reaction barriers for the S=2 N_2O coordinated structures.

Table A.1: Table of Fe-O and O-N distances for N_2O coordinated structures. All distances are reported in Angstroms(Å).

Struct.#	**Fe-O Dist.**	**O-N Dist.**	**Struct.#**	**Fe-O Dist.**	**O-N Dist.**
1	2.34	1.20	32	2.41	1.20
2	2.38	1.20	33	2.35	1.20
3	2.34	1.20	34	2.31	1.20
4	2.59	1.20	35	2.16	1.20
5	2.66	1.20	36	2.41	1.19
6	2.31	1.20	37	2.28	1.20
7	2.39	1.20	38	2.18	1.20
8	2.48	1.20	39	2.36	1.20
9	2.44	1.20	40	2.29	1.20
10	2.71	1.20	41	2.21	1.20
11	2.32	1.20	42	2.20	1.20
12	2.45	1.20	43	2.18	1.20
13	2.12	1.20	45	2.31	1.20
14	2.58	1.20	46	2.25	1.20
15	2.40	1.20	47	2.12	1.20
16	2.25	1.20	48	2.11	1.20
17	2.25	1.20	49	2.12	1.20
18	2.23	1.20	50	2.24	1.20
19	2.48	1.20	51	2.13	1.20
20	2.47	1.20	52	2.13	1.20
21	2.74	1.19	53	2.41	1.19
22	2.60	1.20	54	2.34	1.20
23	2.48	1.20	55	2.45	1.19
24	2.44	1.20	57	2.16	1.20
25	2.50	1.20	58	2.16	1.20
26	2.44	1.20	59	2.13	1.20
27	2.43	1.20	60	2.09	1.20
28	2.50	1.20	61	2.18	1.20
29	2.47	1.20	62	2.25	1.20
30	2.43	1.20	63	2.52	1.19
31	2.43	1.20	64	2.46	1.20

Table A.2: Mulliken charges on iron for high spin (S=2) cases.

Struct.#	**Fe Charge**	**Struct.#**	**Fe Charge**
1	0.6856	33	0.9194
2	0.6593	34	0.9017
3	0.6480	36	0.1126
4	0.3808	37	0.1910
6	0.6373	38	0.3104
7	0.5709	39	0.3527
8	0.5284	40	0.6034
9	0.5338	41	0.8292
10	0.2412	45	0.1722
11	0.6569	46	0.4304
12	0.5786	47	0.5641
15	0.6107	48	0.6843
20	0.5461	49	0.8139
21	0.4593	50	0.5505
22	0.5175	51	0.8756
23	0.8750	52	0.8777
24	0.6660	53	0.4048
25	0.6757	54	0.6516
26	0.7166	55	0.4480
27	0.6315	59	0.4847
28	0.7253	60	0.7683
29	0.7274	61	0.5780
30	0.7285	62	0.1826
31	0.8866	64	0.1256
32	0.9013		

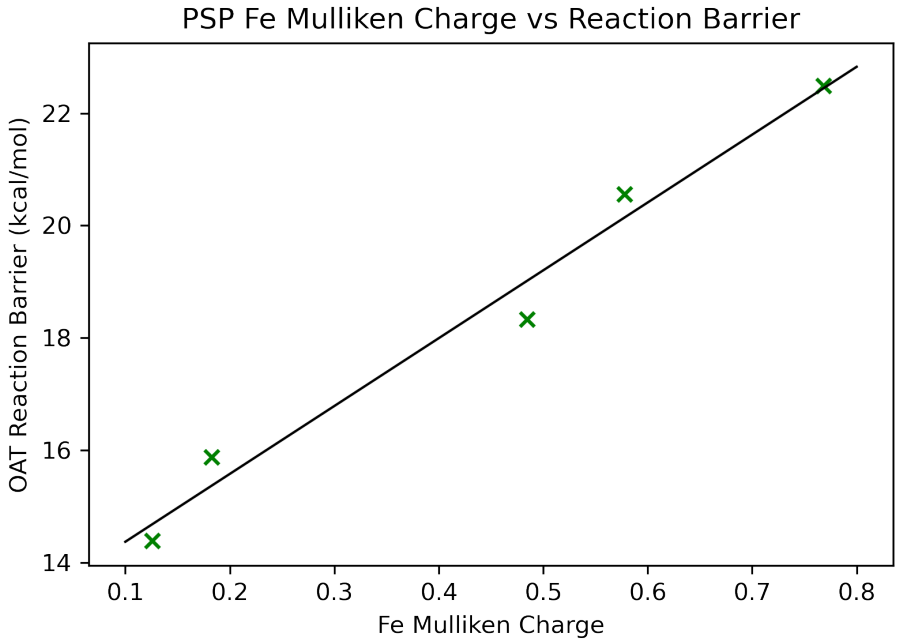

Figure A.10: Mulliken charge on Fe vs reaction barrier of N_2O coordinated psuedo square pyramidal (PSP) structures. RB = 12.08(Charge)+13.16 with $R^2 = 0.9775$

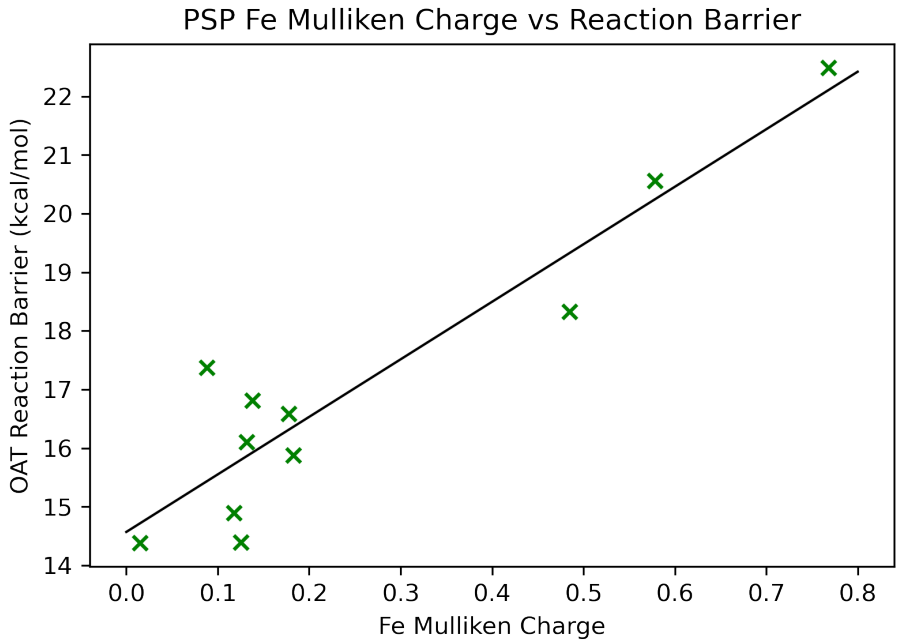

Figure A.11: Fe charge vs reaction barrier of N_2O coordinated psuedo square pyramidal (PSP) structures including auxiliary cases. RB = 9.814(Charge)+14.57 with $R^2 = 0.8626$

Vita

Born in St. Joseph, Michigan, Tobias Robertson spent the most time living in Berrien Springs, Michigan prior to moving his studies at the University of Tennessee Knoxville (UTK). He graduated from the Berrien Springs High School and went on to obtain a Bachelor of Science degree in Chemistry from Western Michigan University (WMU). After graduating from WMU he pursued graduate studies in physical chemistry at UTK. During this time he conducted computational chemistry research regarding the use of nitrous oxide as an oxidant during the formation of iron-oxo species.